Particuology 8 (2010) 28–36

Contents lists available at ScienceDirect

Particuology

journal homepage: www.elsevier.com/locate/partic

Jet dispersion and deposition of charged particles in confined chambers

Chao Zhu [a,*], Dawei Wang [a], Chao-Hsin Lin [b]

[a] Department of Mechanical Engineering, New Jersey Institute of Technology, Newark, NJ 07102, USA
[b] Environmental Control Systems, Boeing Commercial Airplanes, Seattle, WA 98124, USA

ARTICLE INFO

Article history:
Received 25 February 2009
Accepted 18 March 2009

Keywords:
Charged particle deposition
Confined chamber
Electric field
Jet dispersion

ABSTRACT

Dispersion and surface deposition of charged particles by gas–solids jets in confined chambers are constantly encountered in many industrial applications such as in electrostatic precipitation and dry powder coating processes. Understanding and control of flow patterns and trajectories of charged particles are important to the optimal design and operation of such devices. In this study, modeling of flow fields and particle trajectories of dilute gas–solid two-phase flows with charged particles in confined chambers is performed. The dilute gas–solid two-phase flows are simulated by use of a hybrid Eulerian–Lagrangian approach with the one-way coupling between the gaseous phase and particle phase. The space charge distribution is included as a source term in equations of motion or Lagrangian equation of charged particles, which in turn depends on the particle trajectories that determine the space charge distribution. Our modeling predictions suggested that the electrostatic charge plays a significant role in particle radial dispersion. Effect of voltage has limited influence on particle trajectories however it can have a big impact on the residence time. Cone angle has a significant effect on the structure of flow field. For cone with a larger cone angle (typically over 15°), there will be a flow separation along the side wall near the flow entrance region. By comparing with the conical chamber, the cylindrical chamber has a big vortex and three smaller vortexes in the lower part of the chamber, which would complicate the particle dispersion with or without the coupling of charging.

1. Introduction

The phenomenon of the electrification of solid particles is complex. In gas–solid flows, surface contact by collisions, ion collection, and thermionic emission are known to be the major modes of particle electrification.

Electrostatic deposition is widely utilized in many industrial applications, such as the office copying machine that requires precise deposition of ink particles on predefined spaces, electrostatic precipitators that remove charged aerosols from the gas streams, and drug distribution processes which utilizes electrostatic principles to convert a bulk drug powder into a finished dosage form (i.e., a "tablet" or "capsule"). The gas–solid flow field can be significantly affected by the electrostatic forces induced by the charge-carrying particles. Charged particles thus migrate to the collecting plate due to the Coulomb force as well as under the influence of momentum interaction with the gas flow in terms of aerodynamic drag (Choi & Fletcher, 1998).

The phenomenon of turbulent particle dispersion in electrostatic precipitators has been widely investigated. The motion of charged particles suspended in the gas stream was previously studied without considering the effects of particulate space charge (Meroth, Rastogi, & Schwab, 1996; Watanabe, 1989), which can significantly change the electric potential and the charge density distribution, especially when the particles are heavily loaded. Some other studies (Cristina & Feliziani, 1995) considered the effect of particle space charge in the calculation of electric field and current density distribution while assuming the particle concentration is a simple function of distance from the inlet of gas–solids flow. Choi and Fletcher (1998) investigated the particle motion by strong coupling of hydrodynamic equations of ions, gas and particles with the effects of particle space charges and particle charging process.

In the applications of powder coating, the combination of electric and aerodynamic forces on charged powder particles is specially designed and controlled to improve the film thickness distribution on a grounded substrate or target and to increase the transfer efficiency. Mathematical modeling and numerical simulation approaches of study on electrostatic painting processes are performed to examine the influence of the electric field on the spray pattern (Ali, Base, & Inculet, 1994; Ellwood & Braslaw, 1998;

* Corresponding author. Tel.: +1 973 642 7624.
E-mail address: zhu@adm.njit.edu (C. Zhu).

1674-2001/$ – see front matter © 2009 Chinese Society of Particuology and Institute of Process Engineering, Chinese Academy of Sciences. Published by Elsevier B.V. All rights reserved.
doi:10.1016/j.partic.2009.03.012

Elmoursi, 1989, 1992). While, there are only few publications on the investigation of particle transfer efficiency and particle mass distribution on the substrate (Ye, Steigleder, Scheibe, & Domnick, 2002).

In the drug distribution process, the drug powder is supplied by a powder feeding mechanism to a charging module where a static surface charge is placed on small particles of the drug powder. The charged drug powder is then transported using precisely controlled gas flow to a chamber in which it is dispersed as a cloud. The powder is uniformly dispersed in the chamber by a combination of electrostatic forces and aerodynamic design. The charged drug powder is attracted to the substrate through focusing electrodes and deposited in a pattern of small dots. By accurately controlling the electric field with feedback sensors, the system deposits precise amounts of drug powder in many locations on the substrate simultaneously. Thus, the motion of particles is not only affected by the electric field and charge density distribution but also the gas flow pattern which would be heavily influenced by the wall boundary effect of different chamber geometry.

In this paper, a modeling method is introduced for the simulation of a steady-state flow of charged particles within different confined chambers. The effect of different geometry of confined chambers on the particle trajectory is investigated. Effects of charge-to-mass ratio and particle size are illustrated for charged flows in a conical cone deposition chamber with boundary layer jets. Comparative significance between the viscous effect and electrostatic effect within the conditions of this study is also demonstrated.

2. Modeling methodology

Transport and surface depositions of charged powders in confined chambers are complicated by the coupling effects of hydrodynamics, dynamics of particulate flow, and external and/or charge-induced internal electrostatics. When the particle suspension is very dilute, the coupling between the hydrodynamics and dynamics of particle flow can be regarded as one-way coupling. In this case, the particle dynamic behavior is influence by the flow while the fluid flow is independent of the particle behavior. The effects of electrostatics and hydrodynamics on particle movement can be linearly superposed. However, the coupling effect between the particulate flow dynamics and charge-induced electrostatics must be fully considered, which leads to the iterative calculation between the two fields until a converged solution is reached. Hence, in this study, the fluid flow field is independently calculated and considered as pre-determined in the calculation of particle trajectories.

2.1. Modeling objectives and domain consideration

In this study, the flow field and particle trajectories of gas–solid jet with charged particles into confined chambers are investigated. The suspended and charged particles enter the chamber from inlet with the carried gas. With the coupling effect of hydrodynamic and electrostatic forces, the particles are designed to coat onto target plate. The losses of the solids include particles attached to the wall and elutriated into the exhaust gas. The wall boundary of the chamber can be set as grounded, with constant voltage or constant electric density. The collecting plate is grounded so that there is no charge accumulated. To investigate the effect of chamber geometry on the flow field and particle trajectories, two different types of confined chambers, namely, a conical chamber with a divergent angle and cylindrical chamber, as shown in Fig. 1(a) and (b), respectively, are considered. To further study the influence of divergent angle on flow field, two divergent angles (15° and 25°) are selected in the simulation.

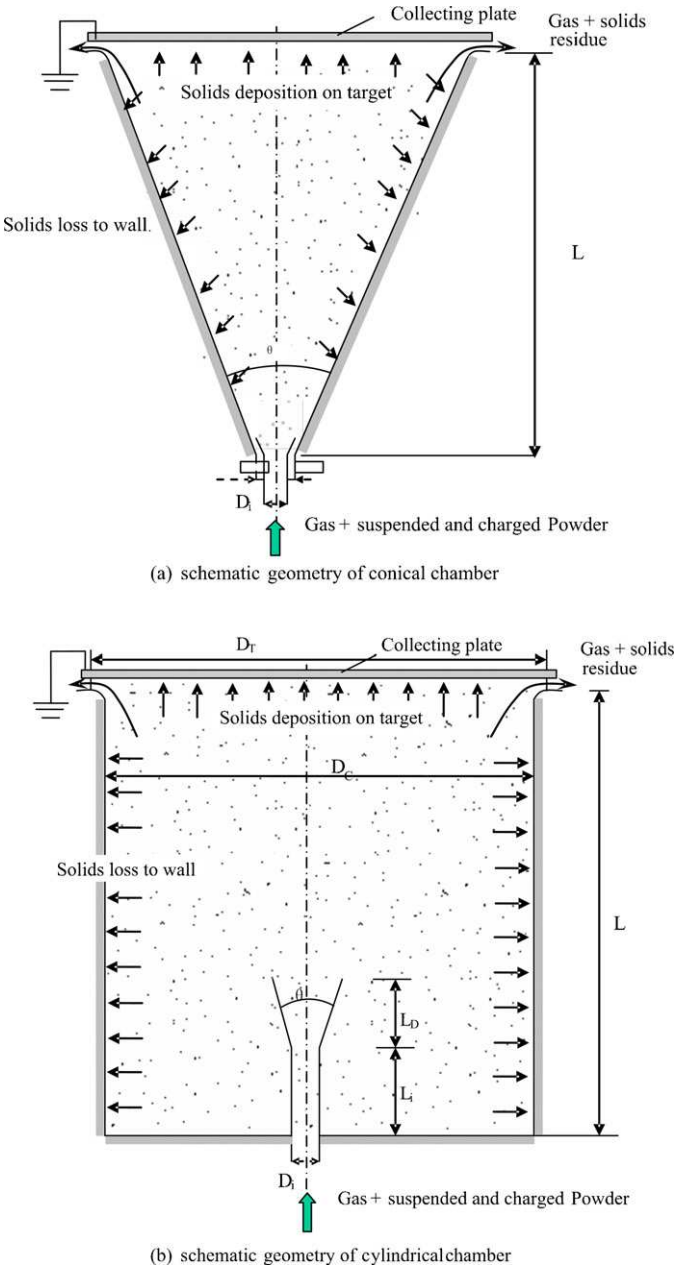

Fig. 1. Schematic diagram of modeling geometry.

2.2. Flow field modeling

The flow is assumed to be incompressible, isothermal, and axisymmetric. The governing equations are the continuity equation and Navier–Stokes equations, which are given as,

$$\nabla \cdot (\rho \vec{u}) = 0, \tag{1}$$

$$\frac{\partial}{\partial t}(\rho \vec{u}) + \nabla \cdot (\rho \vec{u}\vec{u}) = -\nabla p + \nabla \cdot (\bar{\bar{\tau}}) + \rho \vec{g}. \tag{2}$$

The closure problem due to the turbulence transport of the flow is resolved by adopting the standard k–ε model in the

simulation:

$$\frac{\partial}{\partial t}(\rho k)+\frac{\partial}{\partial x_i}(\rho k u_i) = \frac{\partial}{\partial x_j}\left[\left(\mu+\frac{\mu_t}{\sigma_k}\right)\frac{\partial k}{\partial x_j}\right]+P_k+P_b-\rho\varepsilon-Y_M+S_k, \quad (3)$$

$$\frac{\partial}{\partial t}(\rho \varepsilon)+\frac{\partial}{\partial x_i}(\rho \varepsilon u_i) = \frac{\partial}{\partial x_j}\left[\left(\mu+\frac{\mu_t}{\sigma_\varepsilon}\right)\frac{\partial \varepsilon}{\partial x_j}\right]+C_{1\varepsilon}\frac{\varepsilon}{k}(P_k+C_{3\varepsilon}P_b)-C_{2\varepsilon}\rho\frac{\varepsilon^2}{k}+S_\varepsilon. \quad (4)$$

The above equations are solved by using the commercial software FLUENT 6.0 to obtain the flow field of gas phase in the confined chamber.

2.3. Particle trajectory modeling

The trajectory of discrete particles in the flow, which is written in a Lagrangian reference frame, can then be solved by integrating the force balance on the particle. The force balance equates the particle inertia with the other forces acting on the particles, which include the drag force (F_D), the gravitational force (mg) and the electrostatic force (F_e), and is written as

$$m\frac{d\vec{u}_p}{dt}=\vec{F}_D+\vec{F}_e+m\vec{g}. \quad (5)$$

The drag force can be formulated as follows:

$$\vec{F}_D=\frac{1}{2}C_D A\rho\left|\Delta\vec{u}\right|\Delta\vec{u}, \quad (6)$$

where, $\Delta\vec{u}=\vec{u}-\vec{u}_p$ is the slip velocity between the gas and the particle phases; A is front area faced to the flow; C_D is the drag coefficient, which depends on particle Reynolds number and is expressed by

$$C_D=\begin{cases}\dfrac{24}{Re_p} \Leftarrow Re_p\le 2\\ \dfrac{18.5}{Re_p^{0.6}} \Leftarrow 2<Re_p\le 500\\ 0.44 \Leftarrow 500<Re_p\le 2\times 10^5\end{cases}, \quad (7)$$

where Re_p is related to the slip velocity and expressed by

$$Re_p=\frac{\rho_p\Delta\vec{u}d_p}{\mu}. \quad (8)$$

The electrostatic force on particles can be obtained by the electric field and electrostatic charge distributions in the chamber. The electric field with space electrostatic charges is governed by

$$\nabla^2 V=-\frac{\rho_e}{\varepsilon}, \quad (9)$$

where V is electric potential; ρ_e is electrostatic charge density; ε is electromagnetic permeability. It is noted that ρ_e depends on the space distribution of particles and hence is coupled with particle trajectories. The boundary conditions for electric field distribution are:

(i) Wall at a given voltage (or electric potential distribution)

$$V=\text{constant}; \quad (10)$$

(ii) Wall with a given surface charge density distribution

$$\nabla V\cdot\vec{n}=-\frac{\sigma_e}{\varepsilon}, \quad (11)$$

where σ_e is the surface charge density.

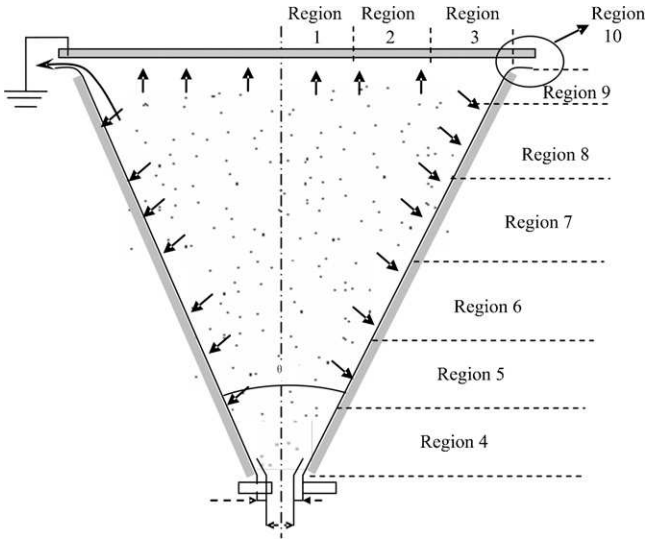

Fig. 2. Region number diagram for particle deposition probability.

Based on Eq. (9) and appropriate boundary conditions, the electric potential V can be solved, which leads to the information of electrostatic field intensity, E, by

$$E=-\nabla V. \quad (12)$$

Moreover, the electrostatic force on a charged particle is given by

$$F_e=Q_e E=Q_e\nabla V, \quad (13)$$

where Q_e is the electrostatic charge carried by an individual particle.

2.4. Particle deposition probability in a predefined region

It is important to estimate the probability of particle deposition in a predefined region. All particle trajectories can be recorded once they reach at the exit or deposit on the wall of the chamber. Therefore, given the distributions of size, charge and velocity of particles at the chamber inlet, the trajectory computation for each group particles can proceed, respectively.

It is assumed that the inlet of duct is randomly filled with particles and is divided into J sub-ring sections with an equal radial interval dR. The probability of a particle placed at R_j, denoted as P_j, would be $2\times dR\times R_j/(R_0\times R_0)$ where R_0 is the inlet radius. The boundary, including the conical wall, ring gap at the exit and the collection plate, can be divided into I regions, based on the prob-

Table 1
Particle collection distributions of 25 μm.

Region	R (m)	Z (mm)	Probability	N_k (no./min)	M_k (mg/min)
1	0–0.05	Top plate	0	0	0
2	0.05–0.10	Top plate	0	0	0
3	0.10–0.128	Top plate	0	0	0
4	Cone wall	7.3–60	0.230	4.216×10^6	70
5	Cone wall	60–120	0.016	2.858×10^5	4.7
6	Cone wall	120–300	0.012	2.205×10^5	3.6
7	Cone wall	300–600	0.045	8.266×10^5	13.5
8	Cone wall	600–863	0.056	1.019×10^6	16.7
9	Cone wall	863–873	0.005	8.403×10^4	1.4
10	Exit	Exit	0.636	1.165×10^7	190

lem to be studied. The probability of the particles collected in every region should be based on a sum of the probabilities of all sized particles that reach the region. A schematic diagram of numbered regions for the conical chamber in our study is shown in Fig. 2. The conical wall, exit and the collection plate are divided into 10 regions with the no. 1–3 on the collection plate, no. 4–9 on the conical wall and no. 10 for the exit. If we denote P_j^i as the probability of finding particles in the boundary Region i that originate from inlet Section j, then the number flow rate and mass flow rate of the particles collected by the ith region are $N_k \times P_j^i$ and $M_k \times P_j^i$, respectively, where M_k and N_k represent respectively the mass flow rate and the number flow rate of the particles of size k. The probability P_j^i depends on the charged particle trajectories solved from coupled equations and boundary conditions (Eqs. (5)–(13)). A sample of particle deposition distribution probability is shown in Table 1.

3. Simulation results and discussions

To compare the geometric effect on the flow field and particle trajectories, the boundary conditions in the simulation for all the different geometries are set to be the same. The inlet gas volumetric flow rate is 100 L/min. The total mass flow rate of the particles is 500 mg/min, of which for the particles sized 5, 25 and 40 μm are 10% (50 mg/min), 60% (300 mg/min) and 30% (150 mg/min), respectively. The material density of particles is

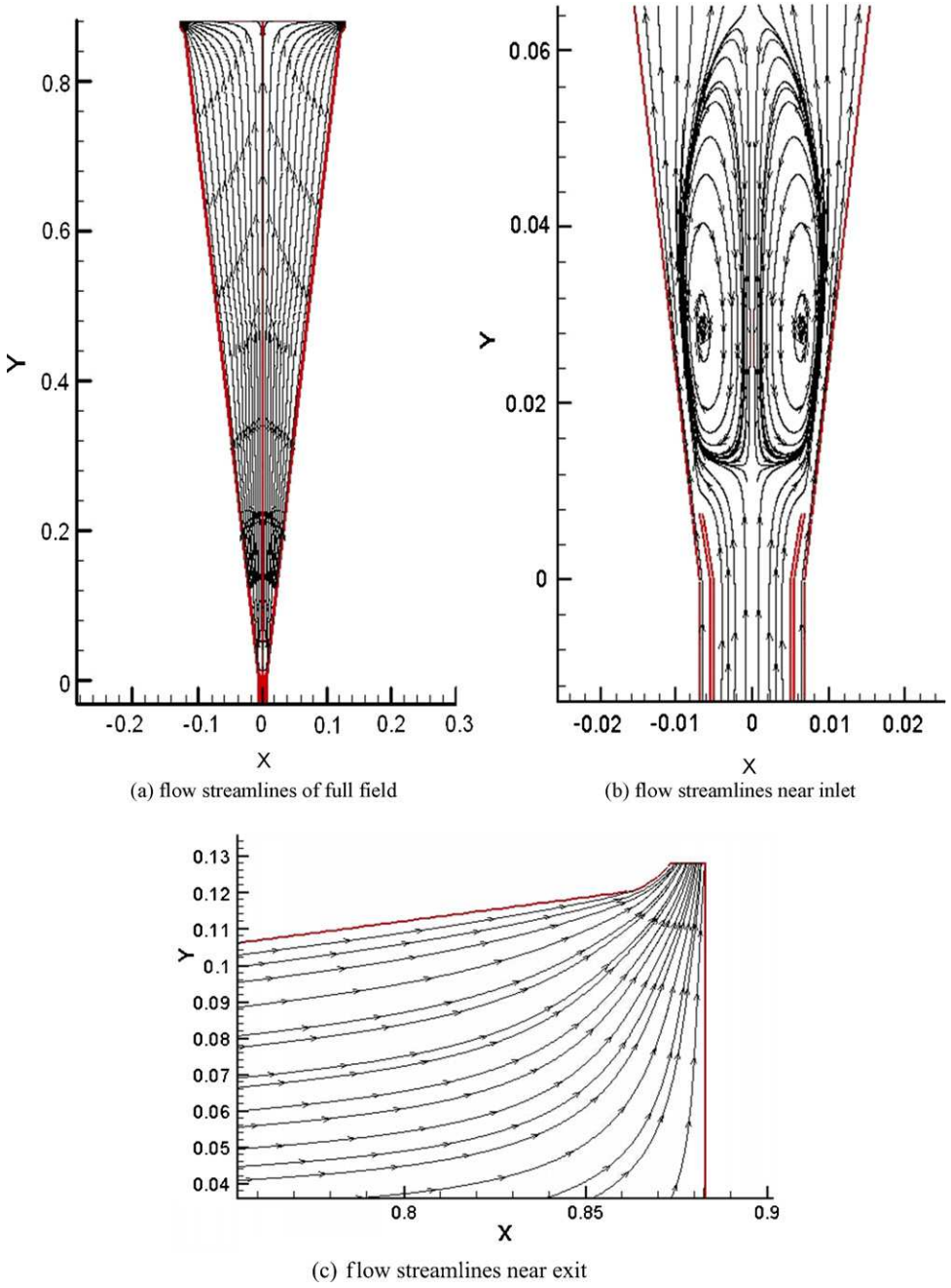

(a) flow streamlines of full field

(b) flow streamlines near inlet

(c) flow streamlines near exit

Fig. 3. Flow streamlines of geometry type 1 (15°).

2000 kg/m^3. The masses of individual particles for 5, 25 and 40 μm are 1.31×10^{-7} mg, 1.64×10^{-5} mg, and 6.71×10^{-5} mg, respectively. Therefore, the number flow rates of particles for 5, 25 and 40 μm are 3.82×10^8/min, 1.83×10^7/min and 2.24×10^6/min, respectively, assuming all particles are spherical.

In the study of polydispersed charged particles, it is assumed that the surface charging densities are the same for all particles. Thus the charge per particle depends on the particle size: 5.52×10^{-15} C (5 μm); 2.57×10^{-14} C (25 μm); 4.11×10^{-14} C (40 μm). For the constant voltage boundaries, $V = 100$ V. For the constant surface charge densities, $\sigma_e = 1.76 \times 10^{-6}$ C/m^2.

3.1. Typical flow field in confined chambers

Typical flow fields are shown in Fig. 3, where the plots of streamline are in the symmetric plane. A noticeable feature is that a central vortex region exists due to the large velocity difference between the main flow and the boundary layer near the wall of the inlet. This vortex will strongly influence the particle trajectories and therefore their depositions downstream.

3.2. Powder trajectories in the absence of electrostatic charges

Calculation of particle trajectories in the absence of electrostatic charges has provided at least three advantages in this study. First, this enables us to estimate the effect of hydrodynamics on the particle trajectory and deposition. Secondly, this can be used later to show the significance of the effect of electrostatic charges on the particle deposition. Lastly, the computed particle trajectories in a charge-free flow usually give a better approximation of an initial charge density distribution in the later calculations of the electric field.

Particle trajectories of each size group are calculated independently due to the dilute suspension condition. Typical particle trajectories are shown in Fig. 4(a)–(c), respectively for particle sizes of 5, 25 and 40 μm. The follow-up characteristics of 5 μm is the best since there is little slip velocity between particles and gas flow. The 5 μm particles go around the vortex. Then all of them go out with the flow at the exit. The 25 μm particles go around the vortex, but part of them reach at the conical wall and the rest move out with the gas flow at the exit. It is noted that the particles of 40 μm go through the vortex. Most of them go out with the gas flow at the exit. Table 1 illustrates the particle collection for the 25 μm particles in ten regions of the chamber.

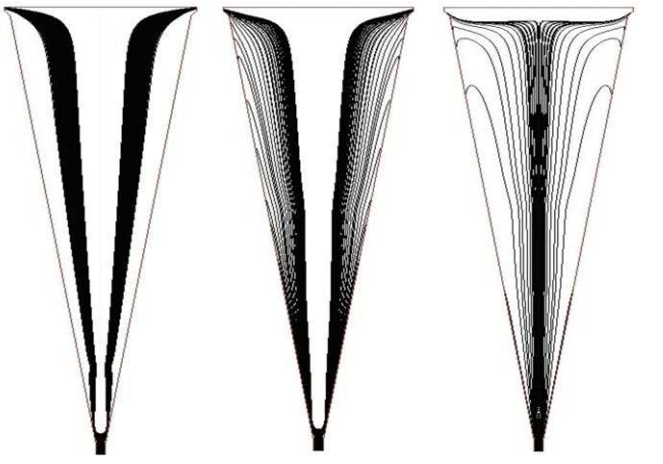

(a) particle trajectories of 5 μm particles (b) particle trajectories of 25 μm particles (c) particle trajectories of 40 μm particles

Fig. 4. Particle trajectories of different sizes without electrostatic charges.

3.3. Charged powder trajectories and electric field intensities

In this study, trajectories of charged particles have been investigated in the chamber with a constant voltage on the chamber wall as well as in the chamber with a constant charge density on the chamber wall. The typical electric intensity distributions are shown in Fig. 5.

The effect of particle size on particle trajectories in a conical chamber with constant electrostatic charge at the wall is shown in Fig. 6(a)–(c). It is shown that the surface charge strongly affects the particles' radial dispersion, which drives particles away from the charged wall. By comparing Fig. 6(b) with Fig. 4(b) (without charges) for 25 μm particles, it appears that electrostatic charge helps in particle deposition on the collection plate as the particles are away from conical wall and fly to the collection plate under the combined effect of hydrodynamic forces and electrostatic force.

3.4. Effect of conical angle

To investigate the effect of the conical angles of the chamber on the flow field and particle trajectories, simulations are carried out on the conical chambers with a divergent angle of 15° and 25°, respectively. The study is performed in the absence of electrostatic forces. The inlet velocities of the air at the inlet of the little tube for the both cases are 35 m/s and velocity distribution at inlet is set to be uniform. Fig. 7(a) and (b) are the enlarged view of flow field near the cone inlet for cone angles of 15° or 25°, respectively. It is seen that there is no separation for the conical flow field of $\theta = 15°$, whereas there exists a flow separation for the cone of $\theta = 25°$.

Fig. 8(a) and (b) shows the particle trajectories in cones of $\theta = 15°$ and 25°, respectively. The red line denotes the conical boundary. The black and blue ones denote the trajectories of particles, with the black ones reaching at the exit and the blue ones reaching the conical wall. The drag force, the gravitational force and the force due to pressure gradient are considered in the particle trajectory model. At $t = 0$ s, particles are released at the tube inlet, with an initial velocity and particle Reynolds number of 0 and 5 m/s, respectively.

3.5. Flow field and powder trajectories in cylindrical chamber

The flow field and powder trajectories in the cylindrical chamber without the effect of electrostatic forces are also investigated. Comparing with the conical chamber with the same gas mass flow rate, the cross-sectional area of the inlet tube and the volume of the cylindrical chamber are bigger, which result in the slower gas flow velocity, say about 0.04 m/s. Moreover, there are a big vortex and three smaller vortexes in the fore section of the cylindrical chamber. The velocities in these vortexes are very small and less than 10^{-3} m/s. Fig. 9 shows the gas flow pattern in the cylindrical chamber.

The typical particle trajectories of 5, 25, and 40 μm are respectively shown in Fig. 10(a)–(c). The flow velocity is high enough to let the particles overcome the gravity for particles of 5 μm. They pass through the chamber and reach at the exit in about 12 s at the speed of 0.04 m/s.

In order to overcoming the gravitational force acting on the 25 μm particles, the relative velocity for the particles should be

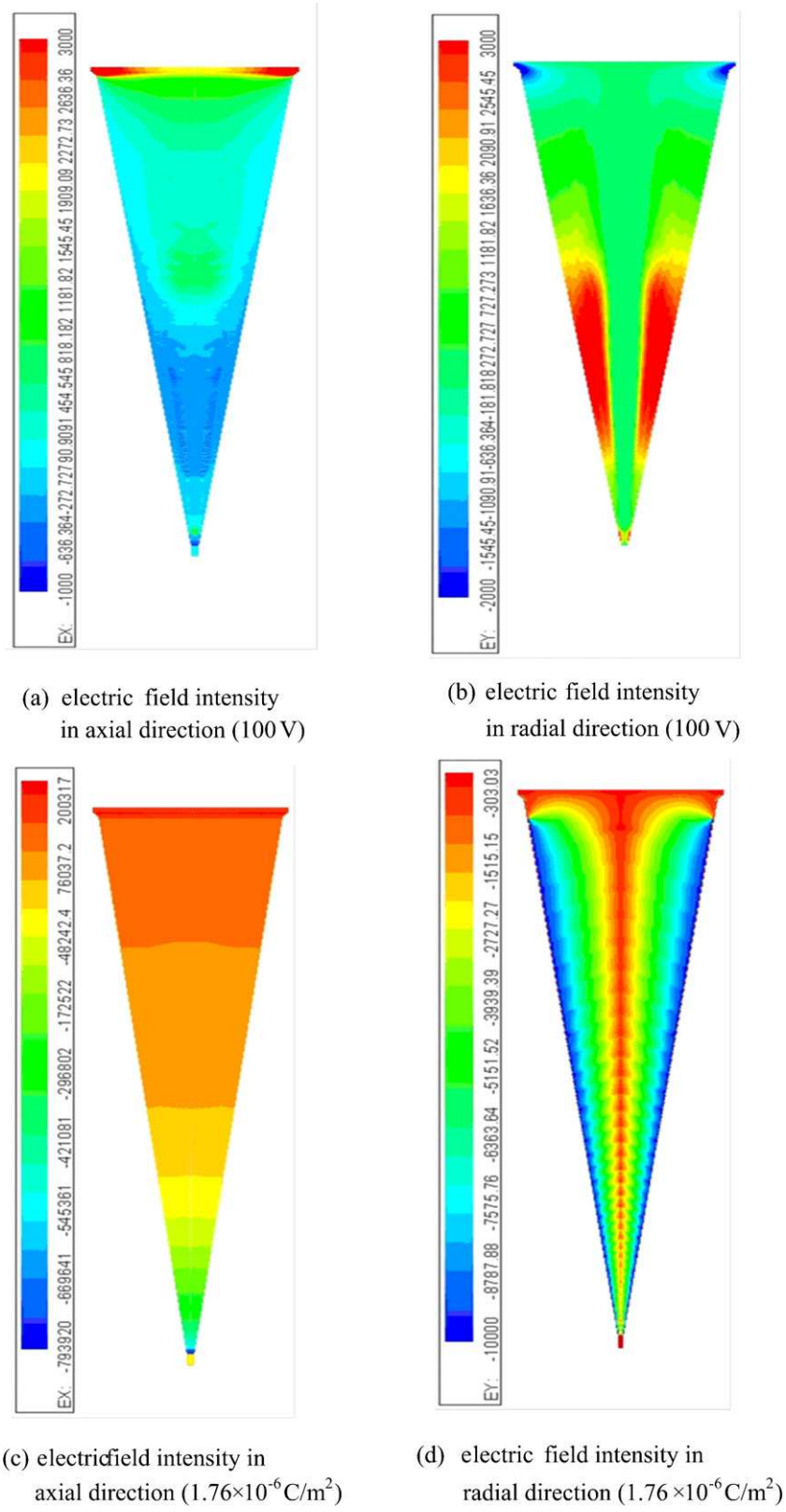

(a) electric field intensity in axial direction (100 V)

(b) electric field intensity in radial direction (100 V)

(c) electricfield intensity in axial direction (1.76×10^{-6} C/m^2)

(d) electric field intensity in radial direction (1.76×10^{-6} C/m^2)

Fig. 5. Electric field intensity (kV/m) at different boundaries (25 μm).

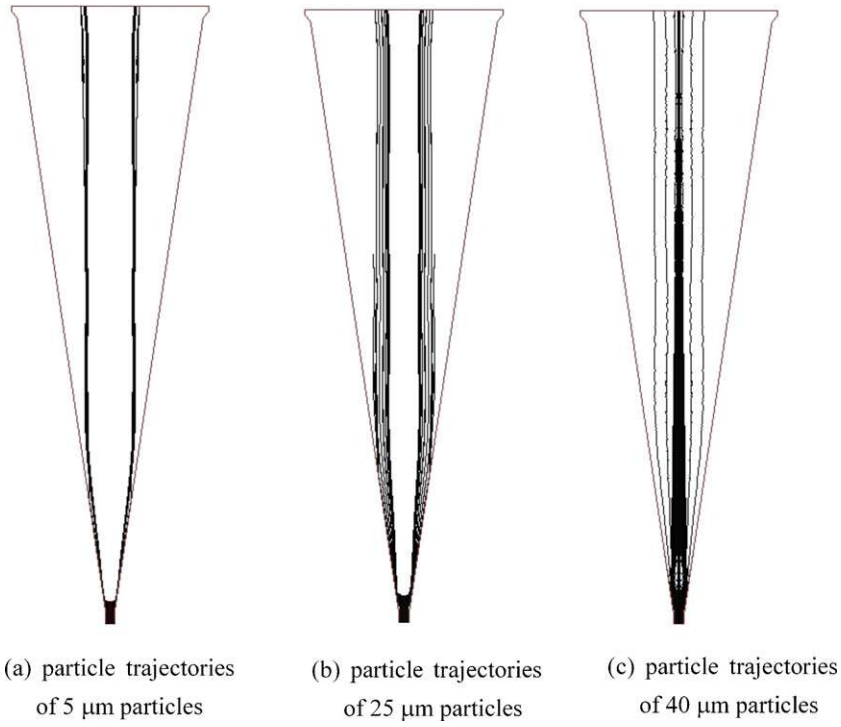

Fig. 6. Particle trajectories with electrostatic charge (1.76×10^{-6} C/m^2).

higher than 0.05 m/s. But as described above, the flow velocity in the chamber is only about 0.04 m/s near the collecting plate. Therefore, the gas flow velocity is not fast enough to carry the 25 μm particles to pass through the chamber. The particles after leaving the inlet section fall into the vortex region due to the gravity and drop back to the lower section of the chamber. Similar to the case of the 25 μm particles, the 40 μm particles exhibit the same behavior, as shown in Fig. 10(c).

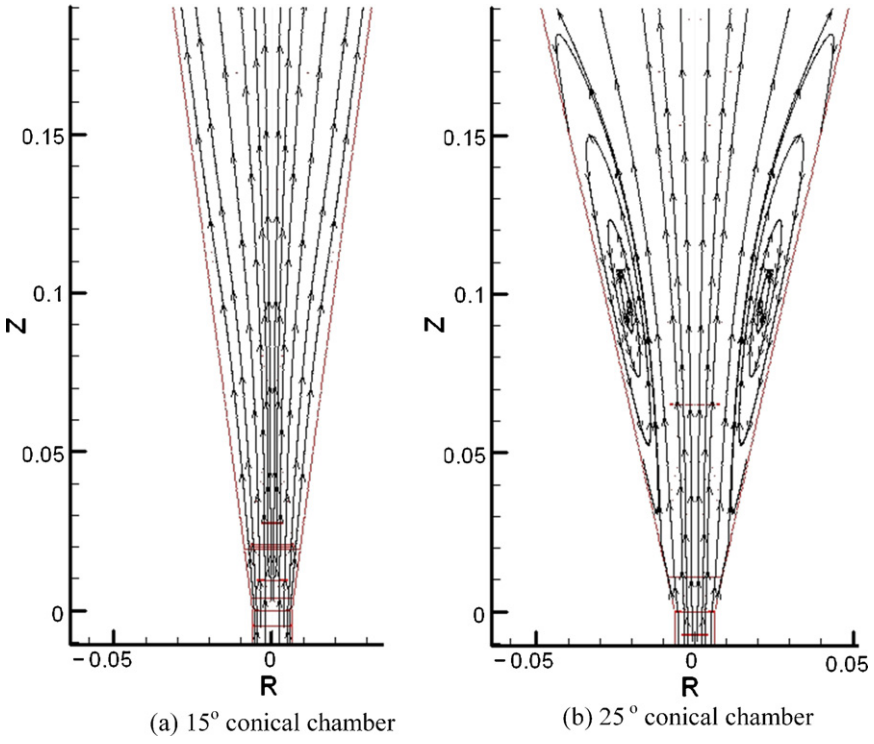

Fig. 7. Flow field near the inlet of conical chamber.

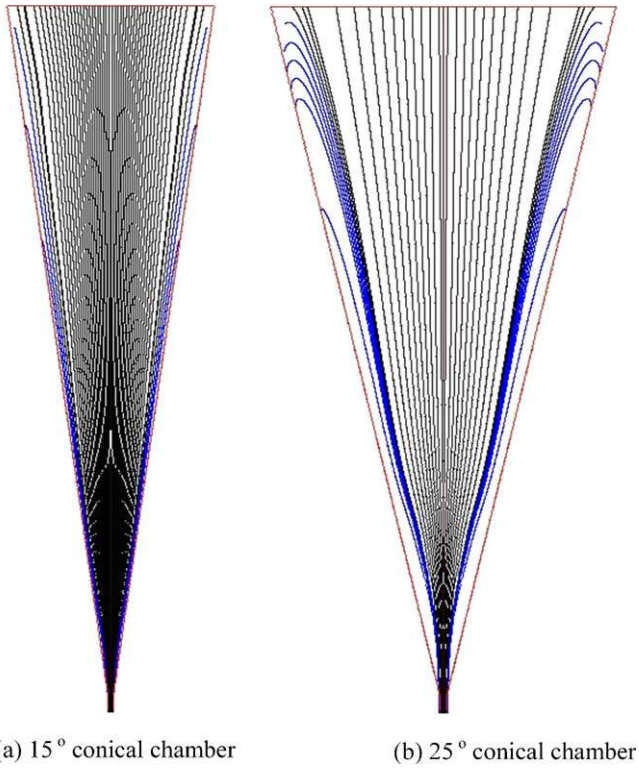

Fig. 8. Particle trajectories in conical chambers with different divergent angles in the absence of electrostatic forces.

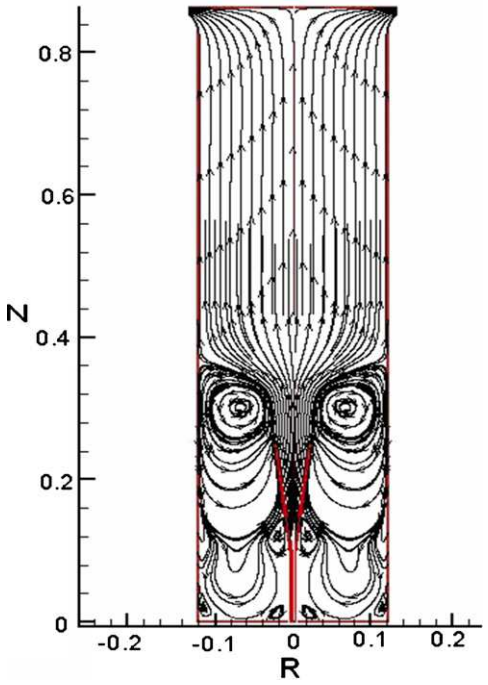

Fig. 9. Gas flow field in cylindrical chamber.

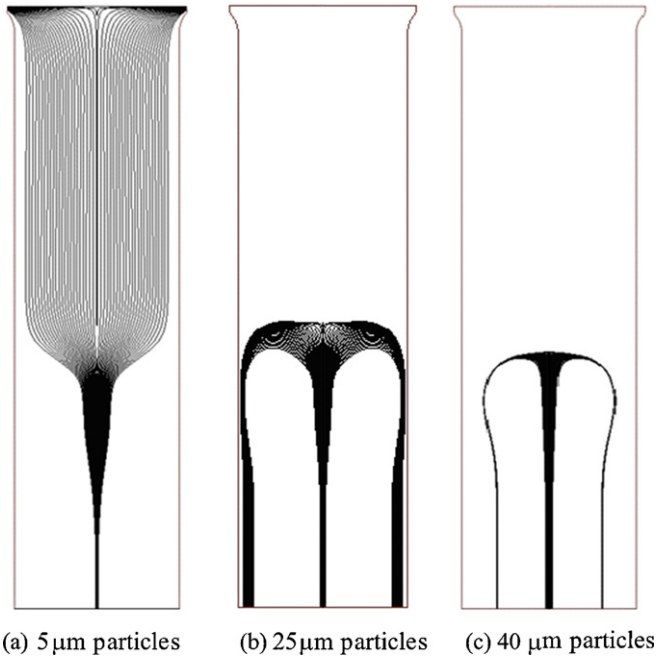

Fig. 10. Particle trajectories of different particle sizes in cylindrical chamber in the absence of electrostatic forces.

4. Conclusions

A complete modeling method has been developed for the study of hydrodynamic and electrostatic deposition of dry powders. The flow field, electric field (including charge-induced electrostatic field), trajectories of polydispersed powders and powder collection probability at a specific wall surface can be simulated. The method has been applied to study the charged particle trajectories and surface deposition in two geometrically different chambers. Our modeling predictions suggested that the smaller particles have better follow-up characteristics of gas flow and can reach to the outlet region by the effect of hydrodynamic forces only. The electrostatic charge plays a significant role in particle radial dispersion. Effect of voltage has limited influence on particle trajectories however it can have a big impact on the residence time. Cone angle has a significant effect on the structure of flow field. For cone with a larger cone angle (typically over 15°), there will be a flow separation along the side wall near the flow entrance region. By comparing with the conical chamber, the cylindrical chamber has a big vortex and three smaller vortexes in the lower part of the chamber, which would complicate the particle dispersion with or without the coupling of charging.

Nomenclature

A	particle front area
C_D	drag coefficient
d_p	particle diameter
D_T	target plate diameter
D_C	chamber diameter
D_i	inlet diameter
E	electrostatic field density
k	kinetic energy
L	chamber length
L_i	nozzle straight section length

L_d	nozzle divergent section length
m	particle mass
p	pressure
P_k	production of kinetic energy
P_b	effect of buoyancy
Q_e	electrostatic charge per particle
Re_p	particle Reynolds number
S	modulus of the mean rate-of-strain tensor
t	time
V	electric potential
x	length
θ	divergent angle
ρ	gas density
$\vec{F}_D$	drag force
$\vec{F}_e$	electrostatic force
$\vec{g}$	gravity acceleration
$\vec{u}$	velocity vector
$\vec{u}_p$	particle velocity vector
$\Delta\vec{u}$	slip velocity
$\bar{\bar{\tau}}$	stress tensor
ε	energy dissipation
μ	kinematic viscosity
μ_t	turbulent viscosity
$C_{1\varepsilon}$	empirical constant
$C_{2\varepsilon}$	empirical constant
$C_{3\varepsilon}$	empirical constant
σ_k	empirical constant
σ_ε	empirical constant
i,j,k	direction subscript
ρ_e	electrostatic charge density
σ_e	surface charge density
ε_e	electromagnetic permeability
$\vec{n}$	direction vector

Acknowledgements

The authors would like to express sincere thanks to Professor Zhichi Zhu of Tsinghua University for his helpful consultation on the modeling approaches, and to Dr. Gui-Hua Qian and Dr. Marty Kashef of Delsys Pharmaceuticals Inc. for their suggestions and discussions on the simulation results.

References

Ali, F. S., Base, T. E., & Inculet, I. I. (1994). Mathematical modelling of powder paint particle trajectories in electrostatic painting. In *IEEE industry applications society, 29th annual meeting* (pp. 1432–1435).

Choi, B. S., & Fletcher, C. A. J. (1998). Turbulent particle dispersion in an electrostatic precipitator. *Applied Mathematical Modelling*, *22*, 1009–1021.

Cristina, S., & Feliziani, M. (1995). Calculation of ionized fields in dc electrostatic precipitators in the presence of dust and electric wind. *IEEE Transactions on Industry Application*, *31*, 1446–1451.

Ellwood, K. R. J., & Braslaw, J. (1998). A finite-element model for an electrostatic bell sprayer. *Journal of Electrostatics*, *45*, 1–23.

Elmoursi, A. A. (1989). Laplacian fields of bell-type electrostatic painting systems. *IEEE Transactions on Industry Application*, *25*, 234–240.

Elmoursi, A. A. (1992). Electrical characterization of bell-type electrostatic painting systems. *IEEE Transactions on Industry Application*, *28*, 1174–1181.

Meroth, A. M., Rastogi, A. K., & Schwab, A. J. (1996). Numerical computation of the turbulent particulated flow in an electrostatic precipitator. In *International symposium on filtration and separation of fine dust* Vienna, Austria, (pp. 994–1001).

Watanabe, T. (1989). Calculation of flyash particle motion and its migration velocity in an electrostatic precipitator. In *Conference record of the IEEE industry application society annual meeting* (pp. 2126–2136).

Ye, Q., Steigleder, T., Scheibe, A., & Domnick, J. (2002). Numerical simulation of the electrostatic powder coating process with a corona spray gun. *Journal of Electrostatics*, *54*, 189–205.